THE JOURNAL OF PHYSICAL CHEMISTRY C
A JOURNAL OF THE AMERICAN CHEMICAL SOCIETY

pubs.acs.org/JPCC

Article

Optimizing Structural and Mechanical Properties of Coiled Carbon Nanotubes with NSGA-II and Reactive Molecular Dynamics Simulation

Ehsan Shahini,* Fazel Rangriz, Ali Karimi Taheri, and Mojtaba Abdi-Jalebi*

Cite This: https://dx.doi.org/10.1021/acs.jpcc.1c00073

Read Online

ACCESS | Metrics & More | Article Recommendations | Supporting Information

ABSTRACT: Coiled carbon nanotubes (CCNTs) have increasingly become a vital factor in the new generation of nanodevices and energy-absorbing materials due to their outstanding properties. Here, the multiobjective optimization of CCNTs is applied to assess their mechanical properties. The best trade-off between conflicting mechanical properties (e.g., yield stress and yield strain) is demonstrated and the optimization of the geometry enables us to find the astonishing CCNTs with a stretchability of 400%. These structures have been recognized for the first time in the field. We derived several highly accurate analytical equations for the yield stress and yield strain by the implementation of multiobjective optimization and fitting a theoretical model to the results of molecular dynamics (MD) simulations. The optimized structures are highly resilient because of two distinct deformation mechanisms depending on the dimensions of CCNTs. For small CCNTs, extraordinary extensibility is mainly contributed by buckling and nanohinge-like deformation with maintaining the inner coil diameter. On the other hand, for large CCNTs, this is accomplished by the creation of a straight CNT-like structure in the inner-edge of the CCNT with a helical graphene ribbon twisted around it. Our work represents an important advance in the design of CCNT based mechanical nanodevices.

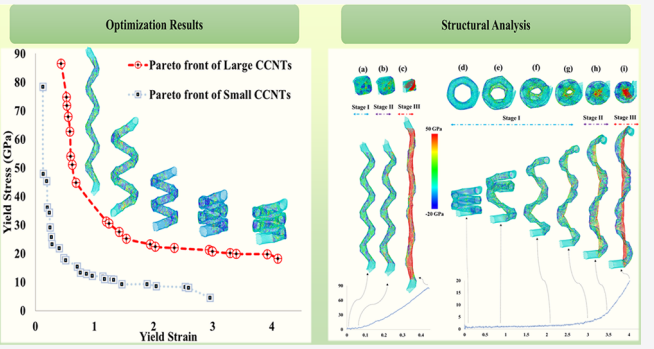

1. INTRODUCTION

The helical shape is a prevalent configuration in the universe from spiraling galaxies to the protein α-helix and DNA double helix. Therefore, it is not surprising that this should also be a common motif observed in carbon nanostructures.[1] Because of their unique 3D helical morphology, relatively high electrical conductivity,[2,3] large surface area,[4] high-performance electromagnetic wave absorption,[5,6] and superelasticity,[7−13] coiled carbon nanotubes (CCNTs) are applicable in a variety of fields such as electrocatalysts for fuel cells,[14−18] supercapacitor electrodes,[19,20] reinforcement,[21,22] biological sensors,[23] hydrogen storage materials,[24,25] and chiral catalysts.[4] In mechanics, the ability of CCNTs to elastically sustain loads at large deflections allows them to store or absorb significant amounts of strain energy. This should render helical CNT reinforced composites applicable where energy-absorbing properties are desired.[26] Thus, to better understand their applications, it is essential to study the CCNT's mechanical behavior. To discover the mechanical properties of CCNTs, a large amount of pioneering experimental and theoretical research was performed.[8,16,35−38,27−34]

Experimentally, Volodin et al.[30] evaluated a Young's modulus of about 0.17 TPa for helical CNT with a coil diameter of 170 nm using atomic force microscopy (AFM). The spring constant and maximum strain of a double-wall CCNT with 126 nm tubular diameter was determined by Chen et al.[39] They clamped the CCNT between the two cantilevers of the atomic force microscope and stretched up to 42% strain. Their results showed a nonlinear springlike stretching response with a spring constant of 0.12 N/m. Hayashida et al.,[27] by using manipulator-equipped scanning electron microscopy (SEM), reported that the elastic modulus of CCNTs varies from 0.04 to 0.13 TPa for coil radii ranging from 72 to 415 nm. Poggi et al.[29] evaluated the compressive strength of CCNTs with different lengths, coil diameters, and number of walls and identified a buckling behavior of multiwalled CCNTs using in situ AFM. Using a continuum model for nanosprings, Yonemura et al.[40] showed stress concentration on the coil wire inner edge. They also confirmed the latter via SEM images showing hollow areas corresponding to the point where fracturing originates. Shang et al.[41] demonstrated the

Received: January 4, 2021
Revised: March 1, 2021

controlled fabrication of spring-like CNT ropes with axial stretchability up to strains of 2.85, stable spring constants, and the ability of energy dissipation during strain cycles. Deng et al.[42] measured Young's modulus of single carbon nanocoils in the range of 5−13 GPa, using an electromechanical vibration technique. Real-time measurements of CNC deformation were conducted by Yonemura et al.[43] to clarify their mechanical responses using a scanning ion microscope. In their results, average CCNT spring constant and tensile strength were evaluated around 1.8 N/m and 100 MPa, respectively. By using the multidimensional force spectroscopy technique, Barber et al.[44] demonstrated unique signatures for buckling, bending, and slip-stick events of the nanocoil under compression. Moreover, the elastic moduli of 13 CCNTs were calculated ranging from 0.4 to 31.4 GPa.

Theoretically, the tensile response of CCNTs of various diameters was investigated at different temperatures.[8] The results of this research have verified that the tension force was reduced by raising the temperature and reducing the diameter of CCNTs. Ghaderi and Hajiesmaili[34] used the molecular dynamics (MD) finite element method to measure the strength and fracture strain of several straight and helical nanotubes with different diameters under the tensile load. Their findings showed that, by increasing the diameter of helical nanotubes, the fracture force is increased while the fracture strain is constant. Feng et al.[35] evaluated the spring stiffness of a three-turn carbon nanospring around 0.36 N/m and a maximum elongation of 38% in the elastic deformation. In another study,[45] the mechanical responses and distributed partial fractures in single- and multistrand helical CNTs with a toughness up to 5000 J/g by MD simulations of tension tests were reported. Shahini et al.[7] studied the effects of temperature and pitch angle on the tensile properties of CCNTs with different chiral vectors. It was found that by decreasing the rising angle, the yield strength and elastic slope decreases while the yield strain, failure strain, and toughness increase. Wu et al.[10] assessed the role of CNT-chirality in their mechanical performances. They reported that for armchair and zigzag CCNTs, the unusual extensibility is accomplished by well-distributed nanohinge-like plastic deformation, whereas for chiral ones this is contributed by superelasticity and nanohinge-like fracture mechanisms. In a recent study, Sharifian et al.[9] studied the effects of geometric parameters on the mechanical properties of CCNTs using atomistic simulations. In the elastic region, they showed CCNTs could resist strain and stress as high as 1.61 and 8.97 GPa, respectively. The tensile characteristics of nanoentwined carbon nanocoil (ECNC) metamaterials were explored by Wu et al.[11] The simulation results showed that the ECNCs imparted a pronounced elastic modulus to the native structures, with a maximum of over 13-fold higher stiffness for one triple helix. In another study,[46] tensile properties of metahelixes composed of perfect CNTs were investigated by means of classical coarse-grained MD simulations. Results showed that mechanical properties such as tensile strength and elastic modulus were strongly dictated by the structural parameters including one- and two-level twisting angles and number of filaments. Table S1 summarizes the results of some experimental and computational research on the tensile test of nanocoils.

In general, it can be concluded that the tensile properties of CCNTs are strongly dependent on the geometry and the chirality of CNTs.[7−11] It should, however, be noted that many questions have remained without any answer regarding the mechanical properties of CCNTs. Due to the complex stress distribution in the tensile test of CCNTs and the infinite number of possible structures, the accurate mathematical expression of mechanical properties as a function of geometrical parameters is not well identified and formulated as yet. Hence, finding structures with excellent mechanical characteristics such as high yield strength and yield strain is not achievable through a process of computational trial-and-error or experimental methods. Moreover, developing accurate theoretical equations between the mechanical properties and morphological variables such as coil and tube diameter, pitch angle, pitch length, and the symmetry of their top view motifs is a vital factor in the mechanical design of CCNTs. The objective of this work is to employ an efficient multiobjective process optimization framework to find the preeminent structures with respect to their mechanical properties. Furthermore, guided by insights from the multiobjective optimization, a continuum model is fitted to the results of MD simulation for developing several accurate analytical equations. Finally, the detailed explanation of the superelastic mechanisms of small and large CCNTs is discussed.

2. THEORETICAL METHODS

2.1. Structural Modeling of CCNTs. Systematic modeling of CCNTs as a function of carbon atoms is an intricate graph-theoretical problem because of their nonlinear helical morphology and existence of non-hexagonal carbon rings. Here, we used the generalized construction scheme of helical CNTs proposed by Chuang et al. with some modifications for our purposes.[47−51] Detailed explanation of structure modeling of CCNTs can be found in the Supporting Information and Figure S1.

2.2. Multiobjective Process Optimization, Pareto Front, and NSGA-II. There are numerous multiobjective optimization techniques. For this work, the nondominated sorting genetic algorithm II (NSGA-II) was used as the optimization algorithm.[52] More descriptions are provided in the Supporting Information (Figure S2). Crowding distance was used as a second-order sorting criterion. NSGA-II creates and fills a mating pool, using binary tournament selection. Then, crossover and mutation operators are applied to certain portions of the mating pool members. Starting from a random geometrical point, the NSGA-II was iteratively applied. The optimization process was halted when no new point was added to Pareto optimal solutions for 10 iterations.

2.3. Molecular Dynamics Simulation. All calculations were carried out in the LAMMPS molecular dynamics simulation package using the AIREBO potential field.[53,54] The many-body short-range REBO force field is capable of modeling the breaking and formation of covalent bonds between carbon atoms during the tensile test. In order to prevent the spurious strain hardening behaviors during tension, the cutoff distance in the switching function of the short-range REBO potential was selected to be 2.0 Å.[55] For the Lennard−Jones potential field, a cutoff radius of 10.2 Å was selected to ensure the application of the potential at large distance. A periodic boundary condition (PBC) was adopted to preclude the edge effects along the axial direction of the helical CNT, and non-PBCs were adopted along two other directions. Before the tensile test, CCNTs were given 50 ps at 300 K to relax in the zero bar pressure condition in the NPT (isothermal−isobaric) ensemble. The pressure and temperature control of the system was performed by using the Nosé−

https://dx.doi.org/10.1021/acs.jpcc.1c00073
J. Phys. Chem. C XXXX, XXX, XXX−XXX

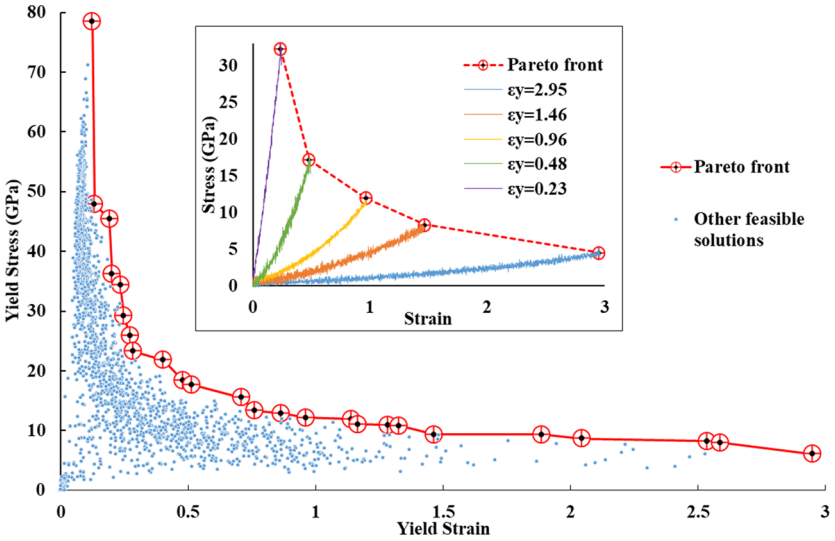

Figure 1. Pareto optimal (red circles) and other feasible solutions (blue dots) for multiobjective optimization of yield stress vs yield strain for small CCNTs. Each point shows a separate nanocoil with unique indices. Most of the solutions have high yield strength while a few of them show superelongation. The inner plot displays the stress−strain curve for five CCNTs from the Pareto front with different yield strains.

Hoover's barostat and thermostat, respectively.[56,57] Time steps of 0.5 fs and the velocity-verlet integration algorithm were adopted to integrate the equation of motions in all simulations. In the tensile simulations, a constant engineering strain rate of 10^9 s^{-1} was applied. During the tension, the NVT (canonical) ensemble and Nosé−Hoover thermostat were used. The tensile stress was calculated using the virial equation.[58−60] As suggested by previous studies, the dissociation of the first atomic bond was considered as the elastic limit of helical CNTs.[7−9] Therefore, the elongation was stopped whenever an atomic C−C bond was dissociated.

3. RESULTS AND DISCUSSION

In this section, the yield stress (σ_y) and yield strain (ε_y) are considered as the objective functions. It is found in our results that CCNTs with large indices dominate the smaller ones due to their superior mechanical properties. To this end, the first four indices which control the size of the CCNTs are divided into two categories. In the first category, the a_1-a_4 indices are selected from the set of integers 1−5. This class of CCNTs possesses small tubes and coil diameters. The second category consists of CCNTs with the first four indices in the range of 5−9. Consequently, the CCNTs are larger, especially in their tube diameters. There is no limitation on the values of the indices, but larger CCNTs increase the computational cost immensely. Additionally, the results can be predicted for larger CCNTs which will be discussed in section 3.3.

3.1. Elastic Behavior of Small CCNTs. The results of the structural optimization for small CCNTs are shown in Figure 1. Each point represents a distinct CCNT with its corresponding yield point values. The Pareto optimal solutions are illustrated in red circles. This figure is revealing in several ways. First, the Pareto front proposes the optimal nanocoils regarding their yield strength and yield strain with the smallest possible dimensions. For example, with careful choosing of the indices, there is a nanohelix that can be elongated up to ε = 2.95 in the elastic region. Second, the relation between σ_y and ε_y in the Pareto front can be defined as a power function by the equation $\sigma_y = k\varepsilon_y^n$, where k and n are constants that are around 10 and −1, respectively. In other words, this result indicates that there is a limitation on achieving mechanical properties of helical CNTs; i.e., if one property (ε_y) increases, the other (σ_y) decreases and vice versa. The other feasible solutions for the $\sigma_y-\varepsilon_y$ optimization are shown in blue dots. Most of the solutions are distributed in strain and stress less than 0.75 and 55 GPa, respectively. This suggests that finding structures that can resist high strains is unlikely. Fortunately, the multiobjective optimization enables us to find those even scarce structures through the crossover and mutation process. The inner plot of Figure 1 presents five stress strain−strain curves of Pareto solutions for different CCNTs. It is readily observed that the stress−strain correlation is almost linear for all kinds of small nanohelixes.

The snapshots of the CCNTs in the inner plot of Figure 1 are shown in Figure 2 at their yield points. The top-view contours of the atomic stress reveal that for all of the nanotubes the majority of the stretching load is absorbed by the inner edges of the CCNTs (Video S1). Since the heptagonal carbon rings are located in this region, in addition to weak binding energy between the carbon atoms in the heptagonal rings, it is more likely that the first bond dissociation occurs in the inner-edge and in heptagonal rings. It is in excellent agreement with experimental observation.[40] Conversely, the outer edge of CCNTs is in either compression or low strain concentration.

Careful observation of Figure 2c−e shows that CCNTs with yield strains larger than 1.0 are characterized by a series of buckling mechanisms. This buckling deformation has also been observed experimentally[29] and predicted via MD simulations before.[8,45] For the structures with superelastic behavior, there are also other mechanisms responsible for this unusual behavior such as the formation of kinks (red arrow in Figure 2c) and elastic "nanohinges" (black arrow in Figure 2c), which remarkably remedy the stress concentration. This behavior was predicted only in the plastic region before.[45]

Upon closer inspection of the top-view snapshots in Figure 2, it is found that the inner coil diameters of CCNTs with high yield strains are maintained while they decrease considerably for low yield strain regimes. Further examination of the inner coil diameter of CCNTs is depicted in Figure 3 and Video S2.

https://dx.doi.org/10.1021/acs.jpcc.1c00073
J. Phys. Chem. C XXXX, XXX, XXX−XXX

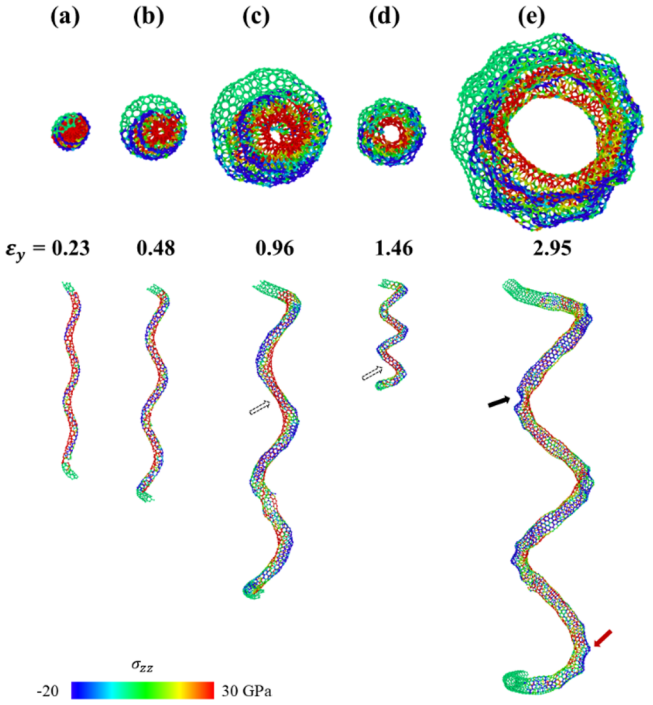

Figure 2. Top- and side-view of the molecular structural configuration of five CCNTs with different yield strains at the yield point. Significant stress concentrations on the inner edge of CCNTs are clearly observed. The arrows indicate the buckling and formation of kinks and nanohinges. The atoms are colored according to von Mises stress.

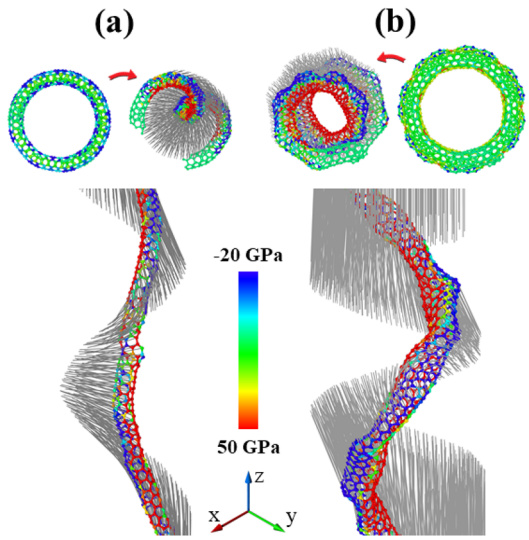

Figure 3. Displacement analysis of middle atoms of two CCNTs with similar initial inner coil diameter but different yield strain. The gray lines show the displacement vectors of atoms during tension. (a) Nanohelix with low yield strain atoms moves horizontally, while in (b) the middle atoms of the CCNT with a high yield strain move in short distances along the load direction. The atoms are colored according to von Mises stress.

Two CCNTs from the Pareto front with similar initial inner coil diameter but different yield strains are selected. The displacement of atoms in gray lines indicates that, for helical CNTs with low yield strain, the middle atoms considerably displaced horizontally in the *XY* plane, while for the other structure the middle atoms moved a short distance along the load direction (z); thus, the nanocoil maintains its inner coil diameter.

3.2. Theoretical Model for the Elastic Region. In order to provide physical insight into the contribution of geometrical parameters on the tensile properties of CCNTs, and to justify the correlation of σ_y-ε_y in the Pareto front, it is beneficial to model a CCNT with an equivalent continuum model. As a first-order estimation, a CCNT can be considered as a thin helical bar with the following governing equations:[61,62]

$$\sigma = \frac{32PR\sin\theta}{\pi d^3}\left(1 + \frac{d}{8R}\right) \quad (1)$$

$$\tau = \frac{16PR\cos\theta}{\pi d^3}\left(1 + \frac{d}{3R}\right) \quad (2)$$

where σ and τ are the normal and shear stresses, P is the axial load, R is the mean coil radius, θ is the pitch angle, and d is the diameter of the coil wire. For small CCNTs, the second term of eq 1 which is $\frac{d}{8R}$ can be neglected. Therefore, the maximum principal stress can be obtained by

$$\sigma_1 = \frac{\sigma}{2} + \sqrt{\left(\frac{\sigma}{2}\right)^2 + \tau^2} \quad (3)$$

As a result,

$$\sigma_1 = \frac{16PR}{\pi d^3}(1 + \sin\theta) \quad (4)$$

Using thermoelastic analysis, it has been numerically shown that appropriately averaged (spatial and temporal) virial stress is the Cauchy stress.[63] Figure S3 shows the six stress components in the tensile simulation of two different CCNTs with low and high pitch angles. Surprisingly, unlike the macroscale engineering springs where the shear stress has the most contribution to the stress tensor,[62] normal stress in the load direction (σ_{zz}) is the only stress component that controls the tensile behavior of nanosprings. As a consequence,

$$\sigma_1 = \sigma_{zz} \quad (5)$$

The total strain in the axial direction for an open-coil spring is calculated by[62]

$$\varepsilon = \frac{64PR^3 l}{d^4\cos\theta}\left(\frac{\cos^2\theta}{G} + \frac{2\sin^2\theta}{E}\right) \quad (6)$$

where l, G, and E are the initial pitch length of the CCNT and the shear and elastic modulus of a CNT, respectively. Substituting P from eq 6 into eq 4, one has:

$$\sigma_{zz} = \frac{dl\xi}{4\pi R^2}\varepsilon_{zz} \quad (7)$$

where ξ is a function of the pitch angle,

$$\xi = \frac{EG\cos\theta(1 + \sin\theta)}{E\cos^2\theta + 2G\sin^2\theta} \quad (8)$$

From eq 7, it can be concluded that CCNTs with high yield strains are characterized by low pitch length, tube diameter, pitch angle, and high coil radius. To shed light on the relation of eq 7 and MD results, the Pareto front structures of small CCNTs are displayed in Figure 4. It can be seen that the structure with the lowest yield strain resembles a straight CNT

https://dx.doi.org/10.1021/acs.jpcc.1c00073
J. Phys. Chem. C XXXX, XXX, XXX−XXX

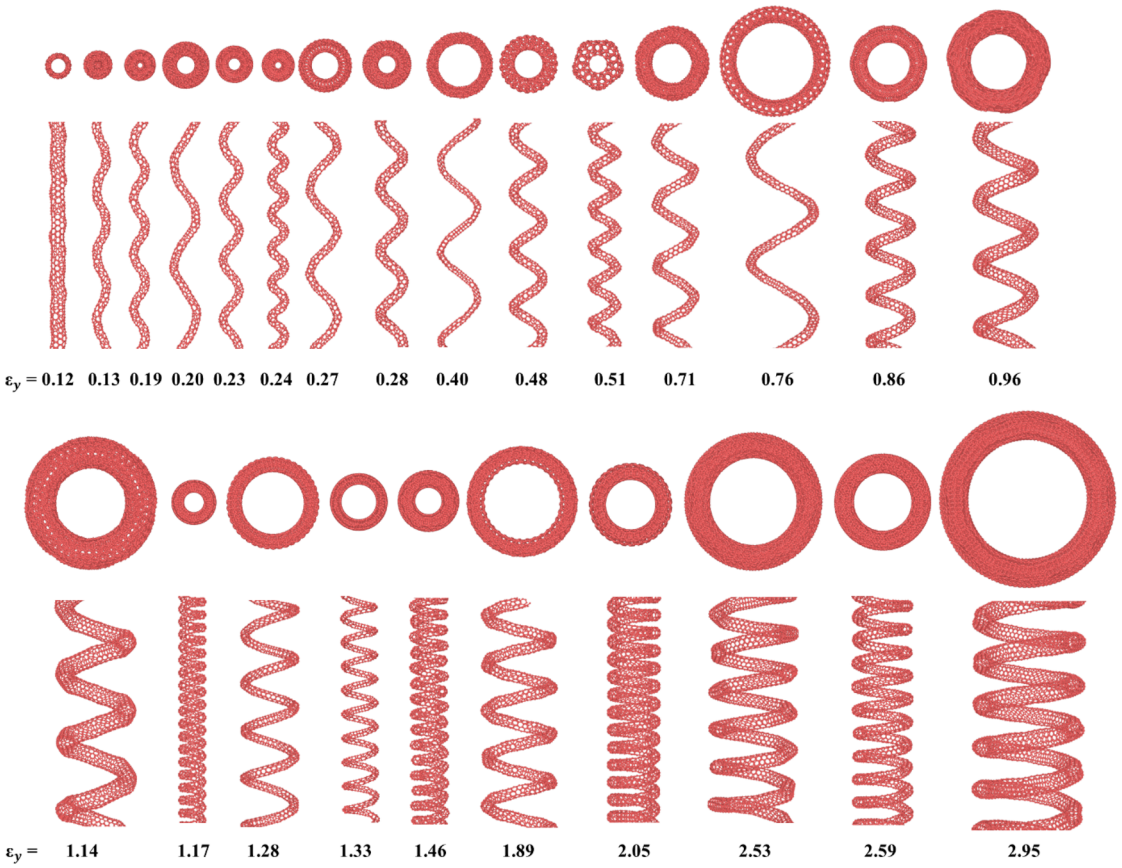

Figure 4. Atomic structure of Pareto optimal solutions for small CCNTs. The yield strain increases from left to right. Overall, by increasing the yield strain, the coil diameter increases while the pitch angle decreases.

Table 1. Structural Parameters and Modulus of Elasticity for the Pareto Optimal Solutions of Small CCNTs

index	d (Å)	l (Å)	R (Å)	θ (deg)	$E_{continuum}$ (GPa)	E_{MD} (GPa)	$E_{modified}$ (GPa)
(2,5,2,5,2,1)	6.48	37.00	22.26	10	1.94	1.84	1.76
(1,3,2,2,2,1)	4.41	16.17	10.01	10	2.85	2.89	2.59
(2,1,2,4,1,1)	4.72	21.36	11.64	10	2.98	3.09	2.71
(2,3,2,5,2,1)	6.25	38.55	16.96	11	3.40	3.26	3.16
(1,2,1,1,1,1)	3.28	16.95	4.87	13	9.71	9.49	9.43
(2,2,1,5,1,1)	4.46	52.49	14.47	15	4.76	4.94	4.82
(1,1,1,2,1,1)	2.56	25.37	6.96	15	5.70	6.85	5.78
(2,1,1,2,1,1)	4.08	14.91	6.64	16	5.93	6.40	6.15
(1,2,2,3,1,1)	4.00	58.87	11.65	19	7.67	8.54	8.50
(3,2,4,5,1,2)	8.45	67.84	15.24	21	11.12	10.48	12.86
(1,3,2,2,1,1)	4.70	47.20	9.01	22	12.39	12.16	14.65
(3,1,2,5,1,1)	6.04	62.46	12.02	23	11.95	12.68	14.44
(2,1,1,4,1,1)	3.86	59.91	8.61	28	14.73	21.93	19.85
(1,1,3,4,1,1)	4.17	125.89	14.16	31	12.52	17.49	18.02
(2,1,1,2,1,2)	4.16	35.73	5.27	32	25.65	34.46	37.74
(1,2,2,2,2,1)	4.02	52.17	6.51	35	23.87	38.40	37.50
(1,1,1,4,1,1)	2.67	110.94	8.23	40	21.06	41.71	36.92
(1,2,2,2,1,1)	4.10	63.48	5.01	45	49.10	81.71	96.02
(1,2,1,1,2,2)	3.60	32.39	2.96	47	62.26	118.00	127.20
(1,2,1,3,1,1)	3.29	93.73	6.06	48	39.03	83.00	81.51
(1,2,1,2,2,1)	3.46	53.75	3.70	53	59.88	145.83	139.51
(1,1,2,4,1,1)	3.22	116.36	4.88	58	64.37	178.70	167.30
(1,2,1,2,1,2)	2.90	59.46	2.75	59	91.70	236.81	243.62
(1,2,1,3,1,2)	3.64	52.01	2.41	64	116.72	361.74	345.95
(1,1,1,5,1,7)	5.80	100.19	1.92	85	124.79	613.44	585.65

https://dx.doi.org/10.1021/acs.jpcc.1c00073
J. Phys. Chem. C XXXX, XXX, XXX−XXX

whereas structures with high yield strains are close-coil nanosprings. Generally, as the yield strain increases, the coil diameter initially increases, then decreases, and finally increases again. As we look at the top-view of CCNTs from left to right in Figure 4, whenever the coil diameter reduces, the other geometrical parameters (e.g., d, l, θ) reduce as well. The reduction of these parameters leads to an increase in yield strain. That is, the amount of these four geometrical variables determines the yield points values.

If the tensile behavior of small nanocoils is considered to be linear in the elastic region, it can be inferred from eq 7 that the elastic modulus of a CCNT is a function of its geometrical parameters. These parameters are detailed in Table 1 for the Pareto front solutions of small CCNTs. The elastic modulus is calculated both from the continuum equation ($E_{\text{continuum}}$) and MD simulations (E_{MD}) and compared in Table 1. Interestingly, for pitch angles less than 35°, there is a satisfactory agreement between the simulation results and eq 7. However, as the pitch angle increases, the difference between E_{MD} and $E_{\text{continuum}}$ becomes larger. This is because at high pitch angles d approaches R and, therefore, the $\frac{d}{8R}$ term in eq 1 is no longer negligible. To deal with this problem, a new coefficient is introduced to eq 7 which is a function of pitch angle. As a result, the modified stress−strain equation in the elastic region of small CCNTs can be obtained by

$$\sigma_{zz} = \frac{dl\xi k}{4\pi R^2}\varepsilon_{zz} \tag{9}$$

where k is the modified coefficient. It is calculated by fitting the continuum model to the MD simulation results,

$$k = 0.73e^{1.254\theta} \tag{10}$$

Figure 5 and Table 1 suggest that analytical equations appear to be well substantiated by the correction factor. However, careful attention must be paid when using eq 9 since it only applies to CCNTs that are in the Pareto front or in the solutions with the rank of less than 8. Furthermore, to gain superelasticity in a nanohelix, having high coil diameter and low pitch angle is necessary but not sufficient. The arrangement of non-hexagonal defects, especially the position of heptagonal carbon rings which absorb the most amount of tensile force, is another factor to be considered. From Table 1, we can find 19 CCNTs with D_{nd} symmetry against only 6 structures with D_{nh} symmetry. Hence, structures with D_{nd} symmetry in their parent TCNT are preferred for small nanocoils.

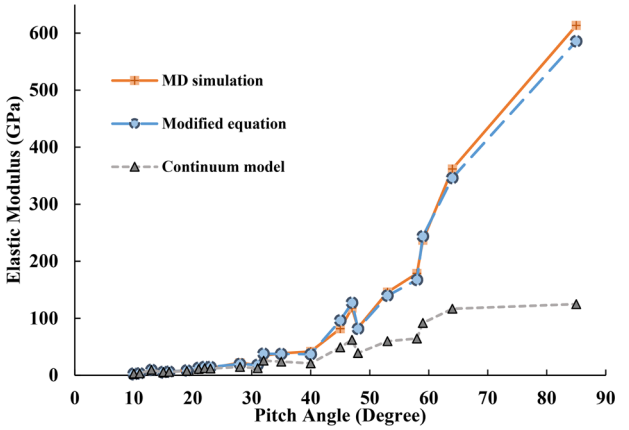

Figure 5. Comparison of the elastic modulus calculated by MD simulations, eq 7, and modified eq 9 proposed in this work. By using the appropriate coefficient, the tensile properties of CCNTs can be expressed as an analytical equation.

As stated previously, the correlation between σ_y and ε_y in the Pareto front solutions can be formulated mathematically by fitting a power function as shown below

$$\sigma_y = 10\varepsilon_y^{-1} \tag{11}$$

Solving eq 9 at the yield point and substituting it into eq 11, one has

$$\varepsilon_y = \frac{2R\sqrt{10\pi dl\xi k}}{dl\xi k} \tag{12}$$

$$\sigma_y = \frac{\sqrt{10dl\xi k}}{2\sqrt{\pi}R} \tag{13}$$

Equations 12 and 13 express the yield stress and yield strain as a function of geometrical parameters and can be used to calculate the highest possible σ_y and ε_y one can obtain in small CCNTs. We observe from Figure 6 that, apart from a slight discordance for strains higher than 2.0, the predicted results from analytical equations are in appreciable agreement with MD results. The prime cause of the discrepancy is the chosen fitting function for the Pareto front. For the sake of simplicity in developing the equations, we used −1.0 instead of −0.86 for the power of ε in eq 11.

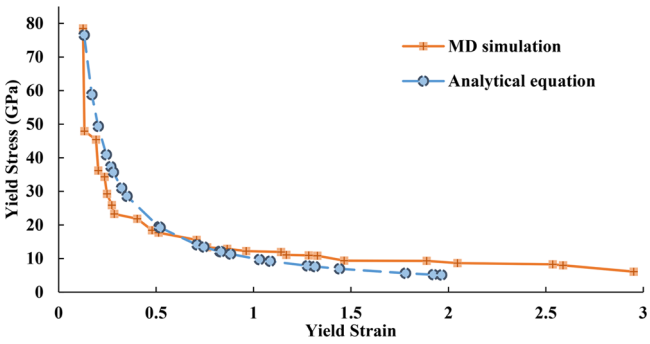

Figure 6. Pareto front resulting from MD simulations in orange squares versus the predicted Pareto front from eqs 12 and 13 in blue circles. The apparent lack of correlation in large strains can be attributed to the simplicity of the fitting function.

3.3. Elastic Behavior of Large CCNTs.

The results of the multiobjective optimization of large nanocoils are shown in Figure 7. In this figure, structures with superelastic behavior can be stretched up to four times their initial length in the elastic region. As far as we know, no one has predicted these amounts of elongation in the elastic region. Similar to small CCNTs, the Pareto front can be fitted to a power function but with higher k and lower n than small ones. To note the similarities and differences between the small and large CCNTs, the Pareto front of small nanocoils is added to Figure 7. It can be seen that the Pareto optimal solutions of large CCNTs have relatively high amounts of yield point values as compared to small CCNTs. This suggests that, by increasing the indices and the size of the nanotube, the mechanical performance improves. Another optimization for nanotubes with indices from 1 to 9 was performed, and the results were

https://dx.doi.org/10.1021/acs.jpcc.1c00073
J. Phys. Chem. C XXXX, XXX, XXX−XXX

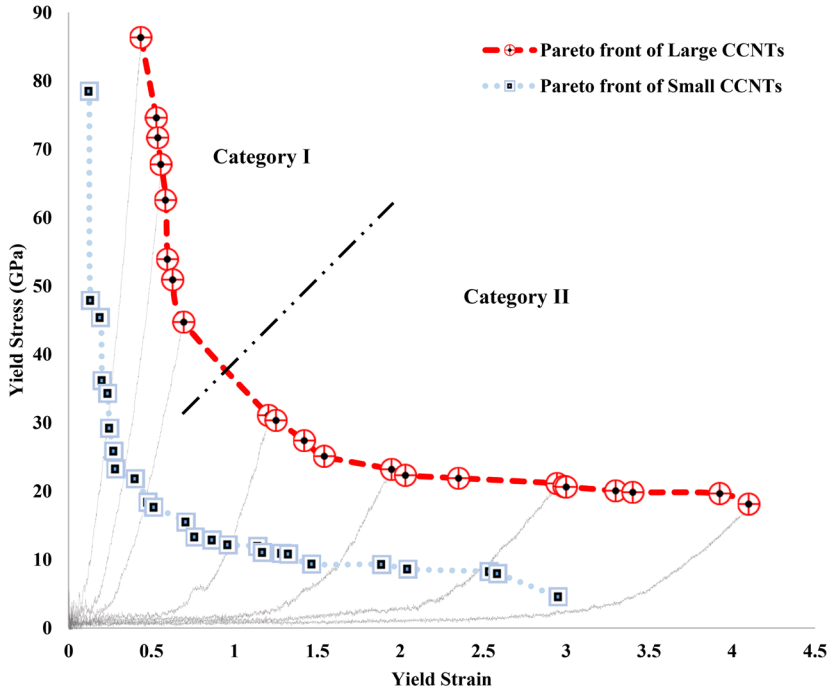

Figure 7. Pareto front for multiobjective optimization of large CCNTs (in red circles). For the sake of comparison, the Pareto front of small CCNTs is also presented in the blue squares. Since the yield point values of large CCNTs are higher than small ones, it can be concluded that the mechanical properties improve as the indices increase.

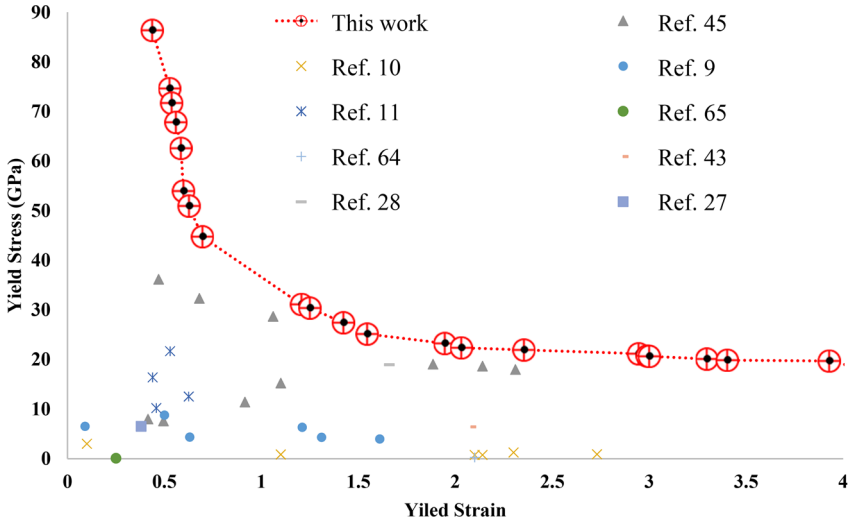

Figure 8. Comparison between the present and previous studies on the tensile behavior of CCNTs in the elastic region. The structures of this work can be elongated 78% higher than previous nanocoils still with higher yield strength.

identical to Pareto optimal solutions of large CCNTs. This means there is no combination of small and large indices that can dominate the CCNTs with large indices.

The yield point values of previous studies and the Pareto front of large CCNTs is shown in Figure 8. This figure confirms that our technique clearly has an advantage over other studies to find CCNTs with high elongation and strength. In the elastic region, CCNTs of this study can be stretched 78% higher than other nanocoils in previous studies. Optimization for large CCNTs regarding their fracture strains showed 22% and 212% improvement compared to previous computational and experimental work,[9−11,35,36,43,45,64,65] respectively.

Figure 9 shows the molecular configurations of Pareto optimal solutions for large CCNTs. It displays a clear trend in the structural parameters as the yield strain increases. As expected and validated by the continuum model, by increasing the yield strain, the radius of coil increases while the pitch length and pitch angle decrease. The tube diameter is almost constant in all structures. The geometrical parameters, yield strength, and yield strain of the Pareto front solutions for large CCNTs are listed in Table 2. From the first column, one can conclude that the first index is between 5 and 7 while the second index is always 5. It indicates that the optimal distance for the heptagonal carbon rings should be 5 units which is approximately equal to 8.1 Å. There is no general trend in the third index, but the fourth index standing for the segment

https://dx.doi.org/10.1021/acs.jpcc.1c00073
J. Phys. Chem. C XXXX, XXX, XXX−XXX

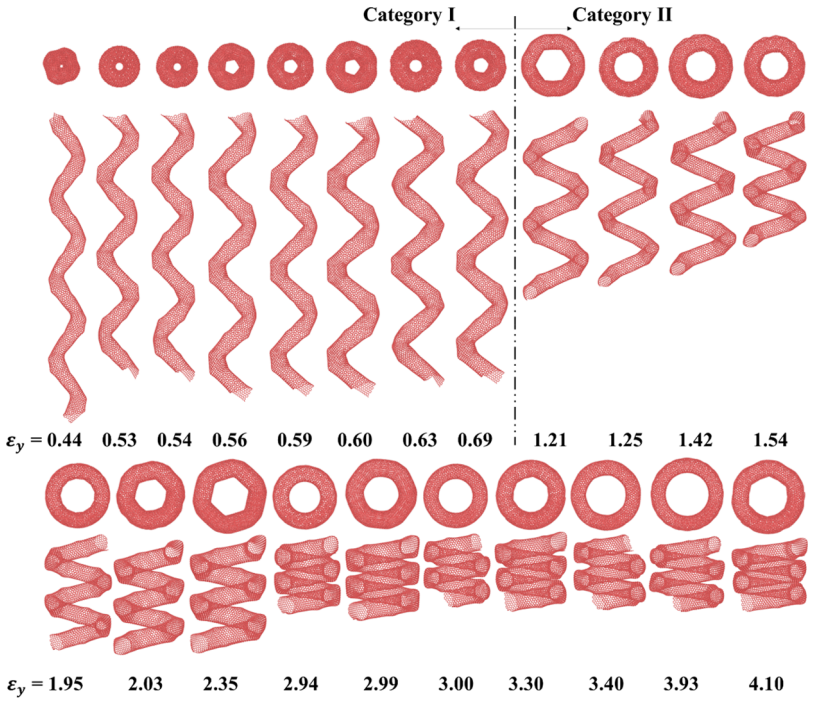

Figure 9. Molecular configuration of the Pareto optimal solutions for large CCNTs. The yield strain increases from left to right. As the yield strain increases, the coil diameter increases and the pitch angle decreases. The morphological transformation between CCNTs with ε_y = 0.69 and ε_y = 1.21 splits the structures into two different categories.

Table 2. Structural Parameters and Corresponding Yield Point Values for the Pareto Optimal Solutions of Large CCNTs

index	d (Å)	l (Å)	R (Å)	θ (deg)	yield strain	yield stress (GPa)	category
(5,5,5,9,2,9)	17.54	178.66	10.58	56	0.44	86.36	I
(5,5,6,8,2,9)	15.95	177.03	12.84	46	0.53	74.63	
(5,5,7,8,2,9)	18.00	180.07	13.01	48	0.54	71.71	
(5,5,8,9,2,8)	17.55	193.57	15.65	46	0.56	67.81	
(5,5,7,9,2,7)	16.64	188.24	15.61	44	0.59	62.59	
(6,5,8,9,2,9)	19.98	187.83	17.26	43	0.60	53.95	
(7,5,5,9,2,9)	19.37	181.83	16.86	40	0.63	50.95	
(6,5,7,9,2,8)	18.20	182.92	17.15	40	0.69	44.76	
(5,5,8,9,2,4)	15.82	147.40	24.80	25	1.21	31.11	II
(5,5,5,9,2,3)	14.45	141.90	22.92	26	1.25	30.38	
(6,5,6,9,2,4)	15.18	131.85	24.41	23	1.42	27.44	
(6,5,6,8,2,4)	15.19	109.42	23.15	20	1.54	25.15	
(5,5,8,8,2,3)	14.73	99.90	25.55	16	1.95	23.23	
(7,5,8,8,2,4)	17.52	92.34	25.69	14	2.03	22.36	
(7,5,9,9,2,3)	18.85	94.95	28.56	13	2.35	21.93	
(6,5,9,7,1,2)	16.13	62.79	24.90	12	2.94	21.16	
(7,5,9,8,1,3)	17.63	68.40	27.49	11	2.99	20.74	
(5,5,9,7,1,1)	15.17	70.08	25.64	12	3.00	20.65	
(6,5,9,8,2,2)	17.15	71.00	27.12	10	3.30	20.09	
(5,5,9,8,1,2)	15.90	75.42	28.53	11	3.40	19.85	
(5,5,8,9,1,1)	16.00	68.46	30.24	9	3.93	19.70	
(6,5,8,9,2,2)	16.59	67.09	29.13	9	4.10	18.14	

length of the CCNT is either 8 or 9 which is in the range of 28.8−31.1 Å. Unlike the small CCNTs, in the large nanohelixes, the D_{nh} symmetry dominates the D_{nd} symmetry and most of the Pareto solutions are from the former symmetry type. The last index which is responsible for the pitch angle reduces by increasing the yield strain.

From Figures 7 and 9 and Table 2 it can be observed that there is a gap between CCNTs with ε_y = 0.69 and ε_y = 1.21 that causes a morphological transfiguration. This change in configuration separates the structures in two different categories. First, the structures with high yield strains that possess high coil radius and low pitch angles. Second, CCNTs with high yield stress which are characterized by low coil radius and high pitch angles. For further investigation of these two types of structures, the stress−strain curves of several CCNTs are exhibited in Figure 7. Referring to this figure, the stress−strain behavior of CCNTs from category I is linear in most part of the tension whereas the pulling stress of other category

https://dx.doi.org/10.1021/acs.jpcc.1c00073
J. Phys. Chem. C XXXX, XXX, XXX−XXX

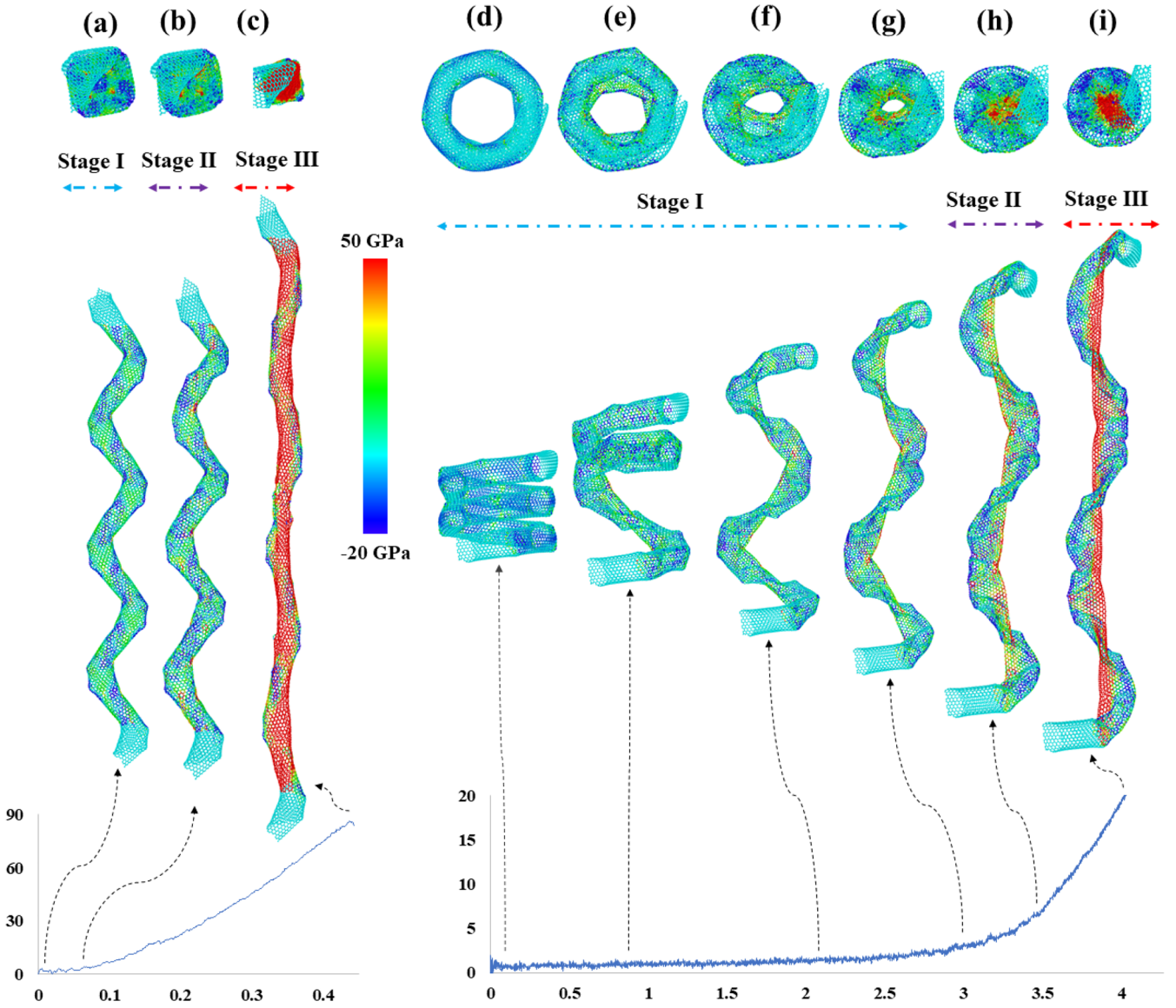

Figure 10. Molecular structural evolution of two large CCNTs from the Pareto front. (a–c) CCNT with the lowest yield strain from category I and (b–i) CCNT with the highest yield strain from category II along with their corresponding stress–strain curves. Atoms are colored on the basis of von Mises stress.

follow a simple power-law function with $k\varepsilon^n$ scaling, where k is a constant proportional to the elastic modulus and n is a constant depending on the geometry.

Overall, the elastic region of all CCNTs from the Pareto front can be divided into three distinct stages. In the first stage, the elastic slope is small and linear and hence the nanocoil can be elongated at relatively low stretching loads. This low-strain stage ceases whenever the stress increases to a critical amount of 3.5 GPa. This stage has the most contribution to the elongation of CCNTs with high yield strains while it is insignificant for nanocoils with low yield strains. A sequence of snapshots of two nanohelixes from both categories is shown in Figure 10 and Video S3. For the first category, this stage is transient but for the second category, this stage contains sequences of vital morphological transformation. First, for the first seven nanocoils with the highest yield strain, because of their small intercoil distance, there exists intercoil van der Waals (vdW) force adhesion that plays a role in the initial elastic loading behavior. The vdW forces cause the reorientation of the coils to follow without any immediate coil separation. With further extensions, the lower turn of the CCNT decoils and the circular cross section of the tube becomes flattened. The other coil is intact until the strain increases to 0.85 and the coil flattening also occurs for this coil. Consequently, all turns are flattened at the strain of 2.13. From this point, the stretching mechanism is the displacement of atoms toward the center in the longitude direction, thus reducing the coil diameter considerably. This stage is ceased after the stress reaches 3.5 GPa. Interestingly, all of these structural transformations occur in relatively low stress where the stress–strain relation is linear. The snapshots of this stage are shown in Figure 10a and d–g.

With further increase in strain, the second stage is commenced. This stage is characterized by the nonlinear increase of tensile stress and a crucial morphological transformation. The displacement of carbon atoms toward the center in the previous stage leads to the generation of a "straight CNT"-like fragment in the inner-edge of the CCNT.

https://dx.doi.org/10.1021/acs.jpcc.1c00073
J. Phys. Chem. C XXXX, XXX, XXX–XXX

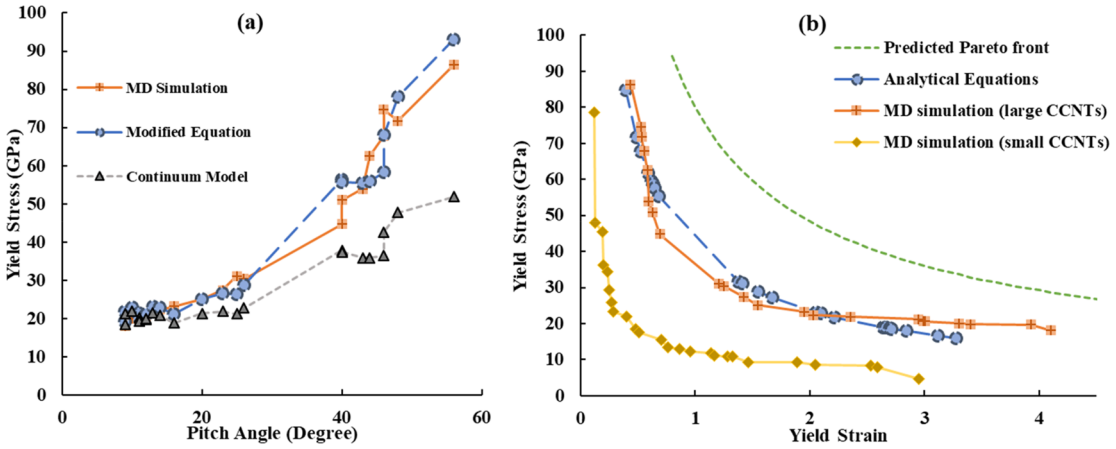

Figure 11. (a) Comparison between simulation and analytical equations of the yield stress as a function of pitch angle for large CCNTs. The modified equation and MD results are in a satisfactory agreement. (b) Pareto front from both MD and analytical equations for small and large CCNTs and predicted Pareto front for CCNTs with indices ranging from 10 to 15.

Hence, the CCNT can be considered as an almost straight CNT with a helical graphene ribbon twisted around it. This stage appears in both categories but lasts longer for nanocoils with high yield strains (Figure 10b and h). In the last stage, the stress increases linearly again but with a higher slope compare to the first stage. This is because the straightening of the inner straight CNT causes significant stress concentrations on the inner-edge of the CCNT and can be observed in Figure 10c and i. This stage extends until a fully straight CNT is generated in the inner part of CCNT and the first atomic bond breaks. By comparison, tensile stiffnesses of nanosprings in this stage are analogous to those of experimentally synthesized ones with a large coil radius.[27,30,66]

The phase transformations in these three stages account for the superelasticity of these materials while the generation of the CNT-like fragment and its stability during tension are responsible for the high yield stress of large CCNTs. To the best of our knowledge, this is the first time that these kinds of phase transformations are predicted in the elastic region. In fact, CCNTs that are not optimized regarding their structures will yield before they show the upper mentioned structural transformations.

Similar to small nanocoils, the analytical equations in the elastic region of large CCNTs is developed by fitting the continuum model to the results of MD simulations. The yield stress for the Pareto optimal solutions resulting from MD simulation and eq 9 are compared in Figure 11a. It can be seen that, after introducing the correction factor, our formula reproduces the response of the large CCNTs in the elastic region. Similar to small CCNTs, the difference between analytical eq 7 and MD results increases by the increase in the pitch angle. Figure 11b compares the Pareto front resulted from MD simulation and analytical equations similar to eqs 12 and 13 after fitting the Pareto front with an appropriate power function. Analogous to small CCNTs, the results are well consistent with MD results except for nanocoils with high yield strains. The results of the multiobjective optimization of small and large CCNTs can be used to predict the larger CCNTs with indices from 10 to 15. They are exhibited with a green dashed line in Figure 11. More details on the correction factor and the corresponding equations for yield stress and yield strain as a function of geometrical parameters can be found in the Supporting Information. Further studies on the multi-objective optimization of CCNTs regarding their ultimate strain and toughness would be interesting and are currently underway in our research group.

4. CONCLUSIONS

Nanoscale helical CNTs have unique mechanical, thermal, and electronic properties that make them suitable for nano-electromechanical systems. This work focuses on employing a multiobjective process optimization framework for optimizing multiple mechanical properties (e.g., yield strength and yield strain) of small and large CCNTs with respect to their geometrical parameters such as coil and tube diameter, pitch angle, pitch length, and symmetry of their top view motifs. The multiobjective optimization results show a reverse relation between yield strength and yield strain which can be fitted to a power function by the equation $\sigma_y = k\varepsilon_y^n$, where n and k are constants and depend on the size of the CCNT. It is found that, by increasing the dimension of CCNTs, mechanical performance improves. The results also confirm that the stretching characteristics of CCNTs are strongly dependent on the geometry. Several theoretical equations are proposed based on fitting a continuum model to the results of reactive MD simulation. The analytical equations can capture the tensile properties of CCNTs in the elastic region. Moreover, a few CCNTs with excellent stretchability in the elastic region are identified. For small CCNTs, the superelasticity of nanocoils in Pareto optimal solutions is attributed to maintaining the inner coil diameter. However, for large CCNTs, the creation of a straight CNT and a helical graphene ribbon is responsible for remarkable elongations.

■ ASSOCIATED CONTENT

Supporting Information

The Supporting Information is available free of charge at https://pubs.acs.org/doi/10.1021/acs.jpcc.1c00073.

Summary of the results of experimental and computational research on the uniaxial tension of CCNTs; structural modeling of CCNTs; multiobjective process optimization, Pareto front, and NSGA-II; effect of strain rate; theoretical equations for large CCNTs (PDF)

Videos for molecular simulation of tensile tests (ZIP)

https://dx.doi.org/10.1021/acs.jpcc.1c00073
J. Phys. Chem. C XXXX, XXX, XXX−XXX

AUTHOR INFORMATION

Corresponding Authors

Ehsan Shahini − *Department of Mechanical Engineering, University of Alberta, Edmonton, Alberta T6G 2R3, Canada;* orcid.org/0000-0003-2696-2059; Phone: +1 5879382114; Email: shahini@ualberta.ca

Mojtaba Abdi-Jalebi − *Institute for Materials Discovery, University College London, London WC1E 7JE, United Kingdom;* orcid.org/0000-0002-9430-6371; Phone: +44 (0)1223 336066; Email: m.jalebi@ucl.ac.uk

Authors

Fazel Rangriz − *Department of Electronic Systems, Norwegian University of Science and Technology, NTNU, NO-7491 Trondheim, Norway*

Ali Karimi Taheri − *Department of Material Science and Engineering, Sharif University of Technology, Tehran 11365-11155, Iran*

Complete contact information is available at: https://pubs.acs.org/10.1021/acs.jpcc.1c00073

Notes

The authors declare no competing financial interest.

ACKNOWLEDGMENTS

The authors would like to thank the research boards at Sharif University of Technology, University of Cambridge, Wolfson College, and Cambridge Materials Limited Company for funding and technical support. We would also like to show our gratitude to Leah Posh, Dr. Masoud Javan, and Dr. Tian Tang for sharing their pearls of wisdom with us during the course of this research.

REFERENCES

(1) Ball, P. *Shapes: Nature's Patterns: A Tapestry in Three Parts*; OUP Oxford, 2009.

(2) Ting, J. M.; Lin, W. C. Unprecedented Re-Growth of Carbon Nanotubes on in Situ Re-Activated Catalyst. *Nanotechnology* **2009**, *20*, 025608.

(3) Geim, A. K.; Novoselov, K. S. The Rise of Graphene. *Nanoscience and Technology: A Collection of Reviews from Nature Journals* **2009**, 11.

(4) Zhang, M.; Li, J. Carbon Nanotube in Different Shapes. *Mater. Today* **2009**, *12*, 12.

(5) Davis, W. R.; Slawson, R. J.; Rigby, G. R. An Unusual Form of Carbon. *Nature* **1953**, *171*, 756.

(6) Qin, Y.; Zhang, Z.; Cui, Z. Helical Carbon Nanofibers with a Symmetric Growth Mode. *Carbon* **2004**, *42*, 1917.

(7) Shahini, E.; Karimi Taheri, K.; Karimi Taheri, A. An Investigation on Tensile Properties of Coiled Carbon Nanotubes Using Molecular Dynamics Simulation. *Diamond Relat. Mater.* **2017**, *74*, 154.

(8) Wu, J.; He, J.; Odegard, G. M.; Nagao, S.; Zheng, Q.; Zhang, Z. Giant Stretchability and Reversibility of Tightly Wound Helical Carbon Nanotubes. *J. Am. Chem. Soc.* **2013**, *135* (37), 13775−13785.

(9) Sharifian, A.; Baghani, M.; Wu, J.; Odegard, G. M.; Baniassadi, M. Insight into Geometry-Controlled Mechanical Properties of Spiral Carbon-Based Nanostructures. *J. Phys. Chem. C* **2019**, *123* (5), 3226−3238.

(10) Wu, J.; Zhao, H.; Liu, J.; Zhang, Z.; Ning, F.; Liu, Y. Nanotube-Chirality-Controlled Tensile Characteristics in Coiled Carbon Metastructures. *Carbon* **2018**, *133*, 335−349.

(11) Wu, J.; Shi, Q.; Zhang, Z.; Wu, H. H.; Wang, C.; Ning, F.; Xiao, S.; He, J.; Zhang, Z. Nature-Inspired Entwined Coiled Carbon Mechanical Metamaterials: Molecular Dynamics Simulations. *Nanoscale* **2018**, *10* (33), 15641−15653.

(12) Coville, N. J.; Mhlanga, S. D.; Nxumalo, E. N.; Shaikjee, A. A Review of Shaped Carbon Nanomaterials. *S. Afr. J. Sci.* **2011**, DOI: 10.4102/sajs.v107i3/4.418.

(13) Tsakadze, Z. L.; Levchenko, I.; Ostrikov, K.; Xu, S. Plasma-Assisted Self-Organized Growth of Uniform Carbon Nanocone Arrays. *Carbon* **2007**, *45*, 2022.

(14) Dunlap, B. I. Relating Carbon Tubules. *Phys. Rev. B: Condens. Matter Mater. Phys.* **1994**, *49* (8), 5643.

(15) Setton, R.; Setton, N. Carbon Nanotubes: III. Toroidal Structures and Limits of a Model for the Construction of Helical and S-Shaped Nanotubes. *Carbon* **1997**, *35*, 497.

(16) Liu, L. Z.; Gao, H. L.; Zhao, J. J.; Lu, J. P. Superelasticity of Carbon Nanocoils from Atomistic Quantum Simulations. *Nanoscale Res. Lett.* **2010**, *5* (3), 478−483.

(17) Lu, M.; Li, H. L.; Lau, K. T. Formation and Growth Mechanism of Dissimilar Coiled Carbon Nanotubes by Reduced-Pressure Catalytic Chemical Vapor Deposition. *J. Phys. Chem. B* **2004**, *108*, 6186.

(18) Ramachandran, C. N.; Sathyamurthy, N. Introducing a Twist in Carbon Nanotubes. *Curr. Sci.* **2006**, *91*, 1503.

(19) Kathyayini, H.; Nagaraju, N.; Fonseca, A.; Nagy, J. B. Catalytic Activity of Fe, Co and Fe/Co Supported on Ca and Mg Oxides, Hydroxides and Carbonates in the Synthesis of Carbon Nanotubes. *J. Mol. Catal. A: Chem.* **2004**, *223*, 129.

(20) Amelinckx, S.; Zhang, X. B.; Bernaerts, D.; Zhang, X. F.; Ivanov, V.; Nagy, J. B. A Formation Mechanism for Catalytically Grown Helix-Shaped Graphite Nanotubes. *Science (Washington, DC, U. S.)* **1994**, *265*, 635.

(21) Du, F.; Liu, J.; Guo, Z. Shape Controlled Synthesis of Cu2O and Its Catalytic Application to Synthesize Amorphous Carbon Nanofibers. *Mater. Res. Bull.* **2009**, *44*, 25.

(22) Bai, J. B. Growth of Nanotube/Nanofibre Coils by CVD on an Alumina Substrate. *Mater. Lett.* **2003**, *57*, 2629.

(23) Cheng, J.-b.; Du, J.-h.; Shuo, B. Growth Mechanism of Carbon Microcoils with Changing Fiber Cross-Section Shape. *New Carbon Mater.* **2009**, *24*, 354.

(24) Bandaru, P. R.; Daraio, C.; Yang, K.; Rao, A. M. A Plausible Mechanism for the Evolution of Helical Forms in Nanostructure Growth. *J. Appl. Phys.* **2007**, *101*, 094307.

(25) Liu, W. C.; Lin, H. K.; Chen, Y. L.; Lee, C. Y.; Chiu, H. T. Growth of Carbon Nanocoils from K and Ag Cooperative Bicatalyst Assisted Thermal Decomposition of Acetylene. *ACS Nano* **2010**, *4*, 4149.

(26) Demczyk, B. G.; Wang, Y. M.; Cumings, J.; Hetman, M.; Han, W.; Zettl, A.; Ritchie, R. O. Direct Mechanical Measurement of the Tensile Strength and Elastic Modulus of Multiwalled Carbon Nanotubes. *Mater. Sci. Eng., A* **2002**, *334*, 173.

(27) Hayashida, T.; Pan, L.; Nakayama, Y. Mechanical and Electrical Properties of Carbon Tubule Nanocoils. *Phys. B* **2002**, *323*, 352.

(28) Volodin, A.; Ahlskog, M.; Seynaeve, E.; Van Haesendonck, C.; Fonseca, A.; Nagy, J. B. Imaging the Elastic Properties of Coiled Carbon Nanotubes with Atomic Force Microscopy. *Phys. Rev. Lett.* **2000**, *84*, 3342.

(29) Poggi, M. A.; Boyles, J. S.; Bottomley, L. A.; McFarland, A. W.; Colton, J. S.; Nguyen, C. V.; Stevens, R. M.; Lillehei, P. T. Measuring the Compression of a Carbon Nanospring. *Nano Lett.* **2004**, *4*, 1009.

(30) Volodin, A.; Buntinx, D.; Ahlskog, M.; Fonseca, A.; Nagy, J. B.; Van Haesendonck, C. Coiled Carbon Nanotubes as Self-Sensing Mechanical Resonators. *Nano Lett.* **2004**, *4*, 1775.

(31) Coluci, V. R.; Fonseca, A. F.; Galvao, D. S.; Daraio, C. Entanglement and the Nonlinear Elastic Behavior of Forests of Coiled Carbon Nanotubes. *Phys. Rev. Lett.* **2008**, *100*, 086807.

(32) Wang, J.; Kemper, T.; Liang, T.; Sinnott, S. B. Predicted Mechanical Properties of a Coiled Carbon Nanotube. *Carbon* **2012**, *50* (3), 968−976.

(33) Ghaderi, S. H.; Hajiesmaili, E. Molecular Structural Mechanics Applied to Coiled Carbon Nanotubes. *Comput. Mater. Sci.* **2012**, *55*, 344−349.

(34) Ghaderi, S. H.; Hajiesmaili, E. Nonlinear Analysis of Coiled Carbon Nanotubes Using the Molecular Dynamics Finite Element Method. *Mater. Sci. Eng., A* **2013**, *582*, 225−234.
(35) Feng, C.; Liew, K. M.; He, P.; Wu, A. Predicting Mechanical Properties of Carbon Nanosprings Based on Molecular Mechanics Simulation. *Compos. Struct.* **2014**, *114* (0), 41−50.
(36) Ju, S.-P.; Lin, J.-S.; Chen, H.-L.; Hsieh, J.-Y.; Chen, H.-T.; Weng, M.-H.; Zhao, J.-J.; Liu, L.-Z.; Chen, M.-C. A Molecular Dynamics Study of the Mechanical Properties of a Double-Walled Carbon Nanocoil. *Comput. Mater. Sci.* **2014**, *82* (0), 92−99.
(37) Zaeri, M. M.; Ziaei-Rad, S. Elastic Behavior of Carbon Nanocoils: A Molecular Dynamics Study. *AIP Adv.* **2015**, *5*, 177114.
(38) Tian, L.; Guo, X. Fracture and Defect Evolution in Carbon Nanocoil - A Molecular Dynamics Study. *Comput. Mater. Sci.* **2015**, *103*, 126.
(39) Chen, X.; Zhang, S.; Dikin, D. A.; Ding, W.; Ruoff, R. S.; Pan, L.; Nakayama, Y. Mechanics of a Carbon Nanocoil. *Nano Lett.* **2003**, *3* (9), 1299−1304.
(40) Yonemura, T.; Suda, Y.; Tanoue, H.; Takikawa, H.; Ue, H.; Shimizu, K.; Umeda, Y. Torsion Fracture of Carbon Nanocoils. *J. Appl. Phys.* **2012**, *112* (8), 084311.
(41) Shang, Y.; Wang, C.; He, X.; Li, J.; Peng, Q.; Shi, E.; Wang, R.; Du, S.; Cao, A.; Li, Y. Self-Stretchable, Helical Carbon Nanotube Yarn Supercapacitors with Stable Performance under Extreme Deformation Conditions. *Nano Energy* **2015**, *12*, 401.
(42) Deng, C.; Li, C.; Wang, P.; Wang, X.; Pan, L. Revealing the Linear Relationship between Electrical, Thermal, Mechanical and Structural Properties of Carbon Nanocoils. *Phys. Chem. Chem. Phys.* **2018**, *20* (19), 13316−13321.
(43) Yonemura, T.; Suda, Y.; Shima, H.; Nakamura, Y.; et al. Real-Time Deformation of Carbon Nanocoils under Axial Loading. *Carbon* **2015**, *83*, 183−187.
(44) Barber, J. R.; Boyles, J. S.; Ferri, A. A.; Bottomley, L. A. Empirical Correlation of the Morphology of Coiled Carbon Nanotubes with Their Response to Axial Compression. *J. Nanotechnol.* **2014**, *2014*, 616240.
(45) Wu, J.; Nagao, S.; He, J.; Zhang, Z. Nanohinge-Induced Plasticity of Helical Carbon Nanotubes. *Small* **2013**, *9* (21), 3561−3566.
(46) Zhao, Y.; Wang, C.; Wu, H. H.; Wu, J.; He, X. Molecular-Dynamics Study of the Carbon Nanotube Mechanical Metahelix. *Carbon* **2019**, *155*, 334−343.
(47) Chuang, C.; Fan, Y. C.; Jin, B. Y. Systematics of Toroidal, Helically-Coiled Carbon Nanotubes, High-Genus Fullernens, and Other Exotic Graphitic Materials. *Procedia Eng.* **2011**, *14*, 2373−2385.
(48) Chuang, C.; Jin, B.-Y. Hypothetical Toroidal, Cylindrical, and Helical Analogs of C_{60}. *J. Mol. Graphics Modell.* **2009**, *28* (3), 220−225.
(49) Chuang, C.; Fan, Y.-C.; Jin, B.-Y. Dual Space Approach to the Classification of Toroidal Carbon Nanotubes. *J. Chem. Inf. Model.* **2009**, *49* (7), 1679−1686.
(50) Chuang, C.; Fan, Y.-C.; Jin, B.-Y. On the Structural Rules of Helically Coiled Carbon Nanotubes. *J. Mol. Struct.* **2012**, *1008*, 1−7.
(51) Chuang, C.; Fan, Y.-C.; Jin, B.-Y. Generalized Classification Scheme of Toroidal and Helical Carbon Nanotubes. *J. Chem. Inf. Model.* **2009**, *49* (2), 361−368.
(52) Deb, K.; Pratap, A.; Agarwal, S.; Meyarivan, T. A Fast and Elitist Multiobjective Genetic Algorithm: NSGA-II. *IEEE Trans. Evol. Comput.* **2002**, *6*, 182.
(53) Brenner, D. W.; Shenderova, O. A.; Harrison, J. A.; Stuart, S. J.; Ni, B.; Sinnott, S. B. A Second-Generation Reactive Empirical Bond Order (REBO) Potential Energy Expression for Hydrocarbons. *J. Phys.: Condens. Matter* **2002**, *14* (4), 783.
(54) Stuart, S. J.; Tutein, A. B.; Harrison, J. A. A Reactive Potential for Hydrocarbons with Intermolecular Interactions. *J. Chem. Phys.* **2000**, *112* (14), 6472−6486.
(55) Shenderova, O. A.; Brenner, D. W.; Omeltchenko, A.; Su, X.; Yang, L. H. Atomistic Modeling of the Fracture of Polycrystalline Diamond. *Phys. Rev. B: Condens. Matter Mater. Phys.* **2000**, *61* (6), 3877−3888.
(56) Nosé, S. A Unified Formulation of the Constant Temperature Molecular Dynamics Methods. *J. Chem. Phys.* **1984**, *81* (1), 511−519.
(57) Hoover, W. G. Canonical Dynamics: Equilibrium Phase-Space Distributions. *Phys. Rev. A: At., Mol., Opt. Phys.* **1985**, *31* (3), 1695−1697.
(58) Subramaniyan, A. K.; Sun, C. T. Continuum Interpretation of Virial Stress in Molecular Simulations. *Int. J. Solids Struct.* **2008**, *45*, 4340.
(59) Clausius, R. XVI. On a Mechanical Theorem Applicable to Heat. *London, Edinburgh, Dublin Philos. Mag. J. Sci.* **1870**, *40* (265), 122−127.
(60) Swenson, R. J. Comments on Virial Theorems for Bounded Systems. *Am. J. Phys.* **1983**, *51* (10), 940−942.
(61) Gere, J. M.; Timoshenko, S. P. *Mechanics of Materials*; Van Nonstrand Reinhold Company: New York, 1972.
(62) Wahl, A. M. *Mechanical Springs*; Second ed.; McGraw-Hill: New York, 1963.
(63) Subramaniyan, A. K.; Sun, C. T. Continuum Interpretation of Virial Stress in Molecular Simulations. *Int. J. Solids Struct.* **2008**, *45* (14−15), 4340−4346.
(64) Wu, T.; Wang, J. N. Carbon Nanotube Springs with High Tensile Strength and Energy Density. *RSC Adv.* **2016**, *6* (44), 38187−38191.
(65) Shang, Y.; He, X.; Li, Y.; Zhang, L.; Li, Z.; Ji, C.; Shi, E.; Li, P.; Zhu, K.; Peng, Q.; Wang, C.; Zhang, X.; Wang, R.; Wei, J.; Wang, K.; Zhu, H.; Wu, D.; Cao, A. Super-Stretchable Spring-Like Carbon Nanotube Ropes. *Adv. Mater.* **2012**, *24* (21), 2896−2900.
(66) Volodin, A.; Ahlskog, M.; Seynaeve, E.; Van Haesendonck, C.; Fonseca, A.; Nagy, J. B. Imaging the Elastic Properties of Coiled Carbon Nanotubes with Atomic Force Microscopy. *Phys. Rev. Lett.* **2000**, *84* (15), 3342.

https://dx.doi.org/10.1021/acs.jpcc.1c00073
J. Phys. Chem. C XXXX, XXX, XXX−XXX